

STEM strain analysis at sub-nanometre scale using milli-second frames from a direct electron read-out CCD camera

K Müller¹, H Ryll², I Ordavo², M Schowalter¹, J Zweck³, H Soltau², S Ihle⁴,
L Strüder⁴, K Volz⁵, P Potapov⁶ and A Rosenauer¹

¹ Universität Bremen, Otto-Hahn-Allee 1, 28359 Bremen, Germany

² PNSensor GmbH, Römerstraße 28, 80803 München, Germany

³ Universität Regensburg, Universitätsstraße 31, 93040 Regensburg, Germany

⁴ Max-Planck-Institut Halbleiterlabor, Otto-Hahn-Ring 6, 81739 München, Germany

⁵ Philipps Universität Marburg, Hans-Meerwein-Straße, 35032 Marburg, Germany

E-mail: mueller@ifp.uni-bremen.de

Abstract. We report on strain analysis by nano-beam electron diffraction with a spatial resolution of 0.5nm and a strain precision in the $4\cdot 10^{-4}$ range. Series of up to 160000 CBED patterns have been acquired in STEM mode with a semi-convergence angle of the incident probe of 2.6mrad, which enhances the spatial resolution by a factor of 5 compared to nearly parallel illumination. Firstly, we summarise 3 different algorithms to detect CBED disc positions accurately: selective edge detection and circle fitting, radial gradient maximisation and cross-correlation with masks. They yield equivalent strain profiles in growth direction for a stack of 5 $\text{In}_x\text{Ga}_{1-x}\text{N}_y\text{As}_{1-y}/\text{GaAs}$ layers with tensile and compressive strain. Secondly, we use a direct electron read-out pnCCD detector with ultrafast readout hardware and a quantum efficiency close to 1 both to show that the same strain profiles are obtained at 200 times higher readout rates of 1kHz and to enhance strain precision to $3.5\cdot 10^{-4}$ by recording the weak 008 disc.

1. Introduction

In transmission electron microscopy (TEM), lattice strain leaves its fingerprint in positions, amplitudes and phases of diffracted beams. Since especially the latter usually depend on lens aberrations as well as on thickness, orientation, and chemical composition of the specimen, phase-exploiting strain measurement via high-resolution [1] or holographic TEM methods [2, 3] can suffer from artefacts due to gradients of these parameters. In contrast, *positions* of diffracted beams are related to lattice plane spacings simply via Bragg's law. In combination with scanning TEM (STEM), strain analysis by nano-beam electron diffraction (SANBED) has become an attractive method with probe diameters of 2.7 nm for parallel beam electron diffraction (PBED [4]) and 0.5 nm for convergent beam electron diffraction (CBED [5]), while strain precision in the 10^{-4} range is comparable. Currently, one severe drawback of SANBED is the limited speed of the CCD detector as a large number of CBED patterns (typically $\sim 10^3$) is to be acquired during the scan. After a brief summary of dedicated algorithms for accurate CBED disc position detection, this article focuses on SANBED using a pnCCD [6, 7, 8] detector which is a low-noise, high-sensitivity and scintillator-free direct electron detection system with kHz readout rate.



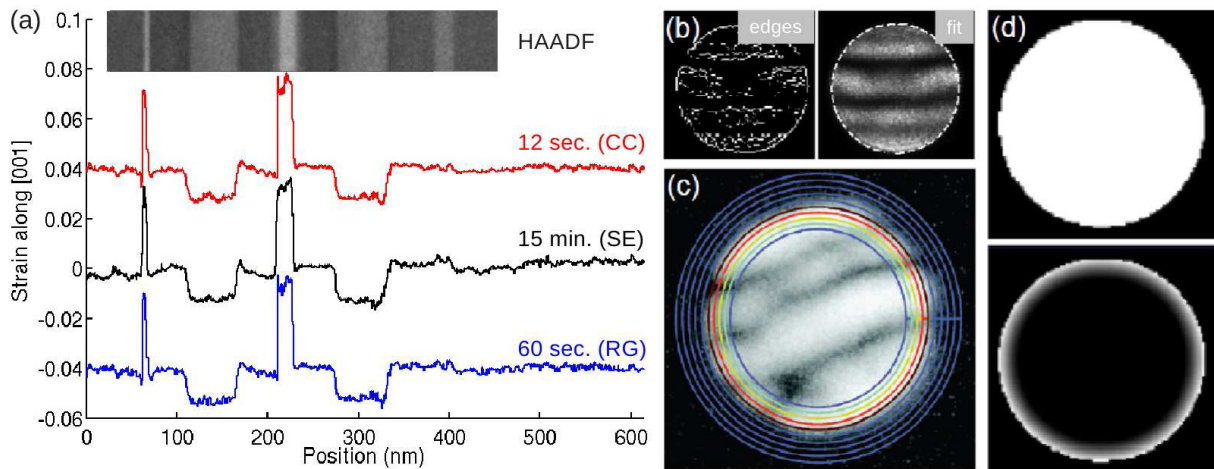


Figure 1. (a) Compressive and tensile strain profiles along [001] measured in a stack of 5 $\text{In}_x\text{Ga}_{1-x}\text{N}_y\text{As}_{1-y}/\text{GaAs}$ layers. The profiles correspond to the 3 algorithms SE, RG and CC with durations of the full evaluation of 800 diffraction patterns also given. (b) 004 disc: initial edges (left) and final circle fit (right) for SE. (c) Rings for inner (coloured) and outer (blue) averages for RG. (d) Full (top) and weighted ring mask (bottom) for CC.

2. Summary of the development of the SANBED method

By focusing the probe with a semi-convergence angle of 2.6 mrad, which we did using an FEI Titan microscope operated in STEM mode at 300 kV, the probe diameter becomes a factor of 5 smaller than in PBED. On the other hand, this requires robust disc position recognition algorithms to cope with the intensity distribution in the CBED reflections which is not only strongly varying inside one disc but also changes drastically among different CBED patterns of one series due to local changes of both thickness and orientation of the specimen. In this study, the sample was 100 ± 10 nm thick, measured in Ref. [5] by high-angle annular dark field (HAADF) STEM.

The first algorithm developed is called *selective edge detection and circle fitting* (SE). Here, Prewitt's edge detection method is applied to raw images yielding edge pixels throughout the full disc as depicted on the left in Fig. 1b. Iteratively, circles are fitted to these edges where the edge pixel with the largest difference from a fit is ignored in subsequent iterations, so that the subset of edge pixels on the disc border finally remains for the last fit on the right in Fig. 1b.

The second algorithm, *radial gradient maximisation* (RG), detects the disc border by maximising the difference between 2 sums: one is calculated from rotational averages inside the disc, one from the outside as shown in Fig. 1c by coloured and blue rings, respectively. During maximisation, position and/or radius of the rings are changed. To stress the disc border, a weighting scheme can be applied to the inner rings as indicated by the different colours.

In a third option called *cross-correlation with masks* (CC), we assume that the CBED disc is similar to an artificial mask so that the relative shift can be calculated by cross-correlation. For the disc-shaped mask in Fig. 1d this is rarely the case due to the inner disc structure in experiment. However, correlating with the weighted ring-shaped mask below stresses the influence of the disc edge and is very robust against such artefacts.

All 3 algorithms have been applied to a sequence of 5 $\text{In}_x\text{Ga}_{1-x}\text{N}_y\text{As}_{1-y}/\text{GaAs}$ layers visible in the HAADF STEM image in Fig. 1a. Given disc positions from SE, RG or CC for all diffraction patterns of a series, strain along [001] is calculated from

$$\mathcal{E}_{[001]} = \frac{R_{004}^0}{R_{004}^0 + \Delta_{004}} \quad (1) \quad \text{or from} \quad \mathcal{E}_{[001]} = \frac{\sin \theta_{004}^B}{\sin(\theta_{004}^B + \frac{1}{2} \Delta \theta_{004})} \quad (2) .$$

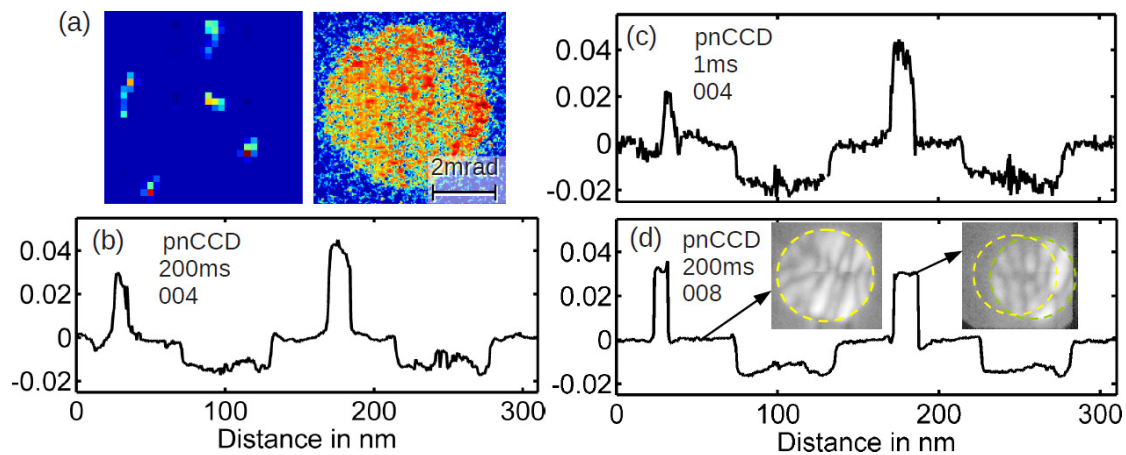


Figure 2. (a) Single electron events at 300 kV (left) and the 004 reflection (right) recorded with the direct electron detector pnCCD. (b) Strain profile as in Fig. 1 but calculated with RG using the 004 disc from pnCCD frames with 200ms frame time. (c) Same as in (b) but with 1 ms frame time. (d) Strain profile calculated with RG from pnCCD frames with 200 ms frame time using the 008 reflection. The two insets demonstrate the high strain sensitivity of 008.

Eq. (1) is valid if both primary and beam 004 are recorded, R_{004}^0 being the average distance between both discs in unstrained GaAs and Δ_{004} being the deviation from R_{004}^0 . In Eq. (2), only one reflection is needed (here: 004) where the Bragg angle θ_{004}^B in unstrained GaAs is taken from literature and angular deviations $\Delta\theta_{004}$ are measured from the disc movement.

The black (middle) graph in Fig. 1a shows the strain profile through the layers in the inset, measured by SE from the 004 reflection in 800 diffraction patterns. It demonstrates that strain in a complex structure with alternating tensile/compressive strain can be determined accurately over a range of more than 500 nm with a precision of $7.3 \cdot 10^{-4}$ being the standard deviation in the GaAs buffer. Best results from the RG and CC approaches have been obtained from logarithmically scaled intensities. The blue (bottom) and red (top) graphs in Fig. 1a show that RG and CC reproduce the SE result with the advantage that the evaluation speeds up by a factor of 15 (RG) or 75 (CC), respectively.

3. Direct electron detection

To take advantage of the SANBED technique in STEM, detectors with a high signal-to-noise ratio, high detection quantum efficiency (DQE) and high-speed readout are needed, especially with respect to 2-dimensional strain mapping. Whereas a conventional scintillator-based CCD camera (Gatan UltraScan 2000) with frame times of 0.5 s has been used to develop pattern recognition algorithms above (Fig. 1), we investigated the performance of a 264^2 pixel, scintillator-free CCD camera, mainly consisting of a pnCCD chip for electron detection and ultrafast readout hardware with technical details described elsewhere [6, 7, 8]. Mounted on an FEI Titan microscope operated at 300 kV at a camera length of 943 mm, we conducted 2 types of experiments:

3.1. Strain analysis with 1 kHz readout rate

The specimen from Fig. 1a has been investigated along a path in growth direction sampled in steps of 0.5 nm with a STEM probe dwell time of 200 ms. Only the 004 disc has been recorded comprising 125 pixels in diameter so that strain was calculated from Eq. (2). A readout rate of 1 kHz was chosen which yields 200 frames of the 004 reflection per scan point so as to check strain results for different frame times afterwards by integrating over 1-200 frames. It is important to notice that, usually, direct

electron detectors for TEM are tuned to high readout rates because this enables single event processing of the traces each relativistic electron causes in the chip as depicted left in Fig. 2a. On the contrary, we nearly saturated the detector in this study to get a complete image of the 004 disc already in a 1 ms frame as shown on the right in Fig. 2a, where single events are impossible to separate. However, as this point spread is isotropic, which we confirmed by Fourier transform of low-dose images [9], it indeed blurs the CBED discs but nevertheless the disc position should remain unchanged.

Because of these substantial differences to scintillator-based CCD images, we first evaluated the direct electron data with comparable frame times of 200 ms (i.e. integration over 200 frames) with the RG algorithm to compare strain precision and -profiles. The result is shown in Fig. 2b which not only reproduces the profiles of Fig. 1a, but also exhibits the same precision of $7.0 \cdot 10^{-4}$. Secondly, we calculated the strain profile in Fig. 2c by using only 1 frame per scan point. Again, the same result is obtained, however, with a lower precision of $1.3 \cdot 10^{-3}$.

3.2. Strain analysis using weak high-order reflections

Finally, we rather aimed at high precision than at high speed and exploited the camera's excellent DQE and signal-to-noise ratio by recording the comparably weak 008 disc with frame times of 200 ms. According to Bragg's law, this reflection is twice as sensitive to lattice parameter changes as 004. This is demonstrated by the two insets in Fig. 2d showing an 008 frame of an unstrained and a strained region, respectively. Consequently, the strain profile in Fig. 2d, obtained with the RG algorithm and Eq. (2) with indices replaced by 008, is characterised by very low noise compared to all other previous measurements. Remarkable precisions in unstrained GaAs have been determined to $3.5\text{--}5.2 \cdot 10^{-4}$.

4. Conclusions

Conceptionally, STEM strain analysis by nano-beam electron diffraction (SANBED) is able to push the spatial resolution of nano-beam-diffraction to the sub-nm range with dedicated algorithms for automated CBED disc position measurement while strain precision is in the range of $4\text{--}7 \cdot 10^{-4}$. In view of the large amount of data recorded in SANBED, cross-correlation with masks is in principle capable of in-situ strain evaluation at the TEM. As to hardware requirements, direct electron detectors such as pnCCD devices with an ultrafast readout unit provide the possibility to either high-speed strain mapping with kHz-readout for 2-dimensional strain analysis, or high-precision strain mapping with high-order reflections. Future tasks could focus on analogous experiments with delay-line detectors, in-situ implementation of SANBED or simulation studies concerning the actual spatial resolution of SANBED at interfaces where regions with different lattice parameters contribute to one diffraction pattern.

References

- [1] Bierwolf R, Hohenstein M, Phillipp F, Brandt O, Crook G and Ploog K 1993 *Ultramicroscopy* **49** 273–285
- [2] Hýtch M, Houdellier F, Hübner F and Snoeck E 2008 *Nature* **453** 1086–1089
- [3] Koch C T, Özdöl V B and van Aken P A 2010 *Appl. Phys. Lett.* **96** 091901
- [4] Béch   A, Rouvi  re J L, Cl  ment L and Hartmann J M 2009 *Appl. Phys. Lett.* **95** 123114
- [5] M  ller K, Rosenauer A, Schowalter M, Zweck J, Fritz R and Volz K 2012 *Microsc. Microanal.* **18** 995–1009
- [6] Str  der L et al. 1997 *Rev. Sci. Instrum.* **68** 4271–4274
- [7] Hartmann R, Buttler W, Gorke H, Herrmann S, Holl P, Meidinger N, Soltau H and Str  der L 2006 *Nucl. Instrum. Methods Phys. Res., Sect. A* **568** 118–123
- [8] Ordavo I et al. 2011 *Nucl. Instrum. Methods Phys. Res., Sect. A* **654** 250–257
- [9] M  ller K, Ryll H, Ordavo I, Ihle S, Str  der L, Volz K, Zweck J, Soltau H and Rosenauer A 2012 *Appl. Phys. Lett.* **101** 212110.